Research Article | Vol. 26, No. 23 | 12 Nov 2018 | OPTICS EXPRESS 30818
Optics EXPRESS

Amplification of flat laser pulse train

A. Hanuka,[1,2,*] J. K. Santucci,[1] D. Edstrom Jr.,[1] L. Schachter,[2] and J. Ruan[1]

[1]Fermi National Accelerator Laboratory, Batavia, IL 60510, USA
[2]Department of Electrical Engineering, Technion-IIT, Haifa 32000, Israel
[*]Adiha@tx.technion.ac.il

Abstract: We present modeling and measurements of flattop amplification of a laser pulse train in a diode pumped Nd:YLF system. We establish a theoretical model, accounting for the transverse Gaussian shape of an amplified laser beam, in order to explain remaining slopes in the pulse train energy. The influence of the transverse Gaussian shape on the train's flatness has been experimentally verified. Based on the model we are able to increase the total amplification of a long train of infrared seed beam in the drive laser system at the Fermilab Accelerator Science and Technology facility. The single-pass amplifier improvements resulted in a gain of ~7 with flat output pulse train for up to 1000 seed pulses.

1. Introduction

High peak power lasers play an essential role in high-field science, requiring a high energy density. One common approach relies upon kilohertz-scale repetition rate laser systems for purely laser-based experiments and research [1]. Recently, higher repetition rate laser systems have been attracting considerable interest for use as drive lasers in photoinjectors [2, 3] as well as other applications that benefit from a MHz-scale repetition rate, such as the generation of widely-spaced frequency combs in the extreme ultraviolet region [4, 5].

One such photoinjector application can be found at Fermilab, which is used to generate short photo-electron bunches to be accelerated through a superconducting RF (SRF) LINAC at the Fermilab Accelerator Science and Technology (FAST) facility. The LINAC consists of a photoinjector, two SRF booster cavities, an ILC TESLA-style cryomodule, multiple downstream beam lines with various diagnostics and a high power beam dump. The primary purpose of this LINAC is to serve as the injector for the new Integrable Optics Test Accelerator (IOTA) [6], but it also provides an opportunity for advanced accelerator R&D beamline-based tests and experiments, such as the planned inverse Compton scattering experiment [7].

The drive laser is based on the one developed for use at the A0 Photoinjector at Fermilab [8], though the gain medium was changed from Nd-doped Glass to Nd:YLF rods, and the flash lamp pumps were changed to fiber-coupled laser diode pumps to get better stability and higher reliability [2].

While short bunch-trains consisting of fewer than 100 fast-repetition rate bunches can be achieved with relative ease to provide a flat intensity distribution through the pulse train, achieving this with a long train like the one the FAST drive laser was designed for, becomes more difficult. Ultimately, the FAST drive laser can achieve a flat intensity distribution through a pulse train of $>$ 1000 pulses at 3 MHz, though this could conceivably also be achieved with a flash lamp pumped system [3].

In this study a theoretical model based on the diode pump is established to explain the experimental data quantitatively. Based on the model we are able to increase the total amplification of a long train of infrared seed beam in the drive laser system at FAST facility. The optimization includes a series of realignments, adjustments of optical components, and pump-diode timing parameters, along with beam spot analysis.

#336263 https://doi.org/10.1364/OE.26.030818
Journal © 2018 Received 4 Jul 2018; revised 16 Aug 2018; accepted 17 Aug 2018; published 8 Nov 2018

Optics EXPRESS

The paper is organized as follows: Section 2 describes the experimental setup and results, and Section 3 presents an analytical model for a train of pulses, as well as simulations results for both radially-uniform and Gaussian beam. Finally, in the discussion (section 4) we suggest simple model which is in excellent agreement with the experimental data.

2. Experimental setup and results

A YLF seed laser from Time-Bandwidth Products GE-100 Series is mode-locked to a harmonic of the 1.3 GHz master oscillator to produce an infrared (IR) seed beam at wavelength λ_s = 1053 nm and pulse rate of 81.25 MHz [9]. The oscillator creates a pulse train with a 3 ps RMS pulse width. These are picked down to 3 MHz (333 ns intrabunch spacing) CW before amplification with a Pockels cell. While capable of producing up to 3000 pulses (1 ms) per train, nominal beam operations typically requires less than 10% of this capacity [9]. This is nominally repeated at a 1 Hz rate, but can be operated at up to 5 Hz (see Fig. 1a).

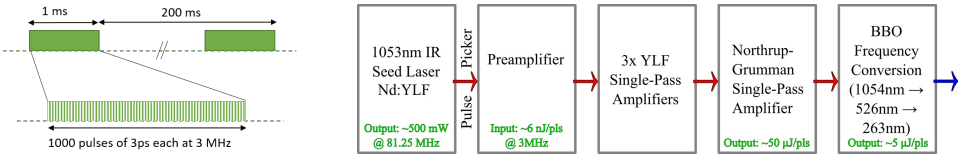

(a) Seed laser pulse structure.

(b) Seven stages of amplification.

Fig. 1. Schematics of the experimental optical layout: (a) Seed laser train macro-pulse (1 ms) consists of 1000 pulses spaced at 333 ns. (b) Seven stages of amplification increase the infrared seed beam energy for higher ultraviolet pulse energies.

Seven stages of amplification increase the infrared seed beam energy for higher ultraviolet pulse energies (see Fig. 1b), which would eventually strike the photocathode to get an electron emission [2]. The chain is broken into three phases: pre-amplifier, three YLF single-pass end-pumped amplifiers, and a commercial amplifier made by Northrop Grumman (NGA) [10]. The latter is a radially pumped single-pass amplifier, which is responsible for the greatest amplification in the drive laser system. After the NGA the seed laser is converted to ultraviolet (263 nm) through two frequency-doubling BBO crystals.

For diagnostics the photodiodes used are Thorlabs DET10A Si biased detectors operating at a few hundred mV, with the intensity controlled through neutral density filters. The seed laser profile, shown in Fig. 2a, was recorded using Prosilica GE1650 Camera, and the beam's RMS radius was 0.08 cm. Both the diagnostics photodiodes and camera are placed at the NGA's exit. Moreover, we monitor the NGA's pump intensity by tracking the diode current (100A), thus non-uniformities in pump intensity are ignored.

Aside from improving the overall gain of the amplifier chain, achieving flat pulse trains (up to 1000 pulses) is a key focus for efficient operation of the drive laser system at FAST. By adjusting the timing of the pump diodes' trigger delays and pulse width, the λ_p = 804 nm pump diode pulses can be better synchronized with the λ_s = 1053 nm seed train pulse. As shown in Fig. 2b, if the delay time between the seed laser (green), and the pump pulse (purple) is long, the first seed laser is more amplified than the following seed pulses. On the other hand, as shown in Fig. 2c, if the delay time between the seed laser and the pump pulse is short, the first seed laser is less amplified than the following seed pulses. Both cases above reach steady state towards the end of the train. However, it is critical to obtain constant output energy per pulse, namely flattened pulse trains. The latter would result in more uniform electron bunch production from the photocathode.

In principle, a long train requires more than a simple delay adjustment (e.g. pump diode modulation) to achieve a flat intensity distribution. However, the closest case we achieved in the

Optics EXPRESS

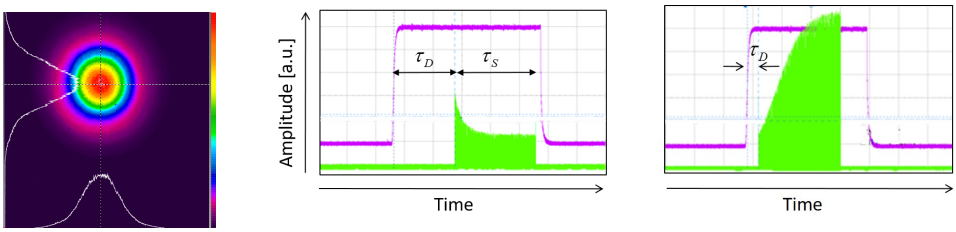

(a) Seed laser profile. (b) Negative train slope. (c) Positive train slope.

Fig. 2. (a) Seed laser profile. The beam's RMS radius is 0.08 cm. (b) Long delay time (τ_D) between the seed laser train τ_S = 333 μs (green) and the pump diode (pink) causes negative slope. (c) Short delay between the seed and pump lasers causes positive slope. Flattened peak can never be achieved by adjusting the diode trigger delay for long train.

experiment for flat output is shown in Fig. 3. The Fig. shows output energy versus time for a train of 1000 seed laser pulses, as captured by the oscilloscope (Agilent DSO6104A). At the beginning of the train (point 1) there is a negative slope, followed by a curvature (point 2), and a steady state region (point 3) is obtained towards the end of the train. In what follows we refer to this case as the curvature on the "flat" output.

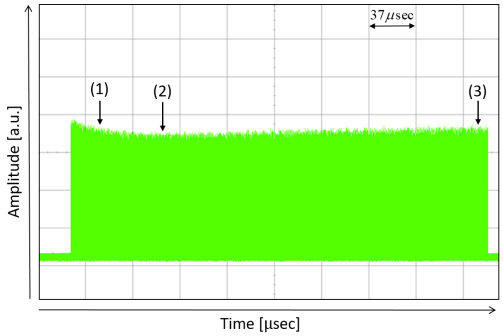

Fig. 3. Output energy versus time for a train of 1000 seed laser pulses, as captured by the oscilloscope. At the beginning of the train (point 1) there is a negative slope, followed by a curvature (point 2), and a steady state region (point 3) is obtained towards the end of the train. Steady state flat output for the whole train can never be achieved for any delay time.

Modeling the laser amplifier is critical for designing and tuning the setup, as well as minimizing the time to first operation. We use a relatively simple analytical model to explain our results. The model may also lay the ground for eliminating the curvature on the flat output. For example, designing a tapered pulse or using a different method such as double pass. In what follows we describe the suggested analytical model for uniform and Gaussian beams.

3. Analytical model

In order to improve the amplifier chain, we simulate the commercial radially-pumped Northrop Grumman Amplifier (NGA). The model assumptions are as follows: (i) full overlap between pump laser (λ_p) and TEM mode seed laser (λ_s); (ii) Constant temperature; (iii) surface reflections and losses due to diffraction and scatter are ignored; (iv) pump rate in the medium is constant both transversely and longitudinally; (v) The seed pulses are short, so that pumping during each single seed pulse is ignored. In other words, we considered pumping in-between two adjacent

Optics EXPRESS

pulses.

Following the model in [10], the rate equation for the number of atoms in excited state, denoted as (n), is

$$\frac{dn}{dt} = W_p\,(n_{\rm tot} - n) - \frac{n}{\tau_{\rm f}} \tag{1}$$

where $n_{\rm tot}$ is the total number of active ions in the pumped medium, W_p is the pump rate, and $\tau_{\rm f}$ is the fluorescence life time of Nd:YLF crystal.

For a train of seed pulses, all of which are amplified by a single pumping event, each pulse is effected by the preceding pulses. Since each pulse in the train removes a fraction of the stored energy, depending on the pump rate and pulse separation, the stored energy may be fully replenished. In this case, a steady state (flat gain) would be achieved for the whole train. Otherwise, if the energy reservoir is not restored between successive pulses, the gain would either decrease or increase within the first few pulses, until it would reach the steady state.

As a result, for the $i-$th pulse, arriving at time t_i, Eq.1 is integrated from t_i until the next pulse arrives at t_{i+1}, with new initial population condition $n(t_i)$. The latter is calculated from the stored energy reduced by the output energy of the amplifier

$$n\,(t_i) = \frac{hc}{\lambda_{\rm s}}\left[E_{\rm stored}\,(t_{i-1}) - E_{\rm out}\,(t_{i-1})\right], \tag{2}$$

where the stored energy is $E_{\rm stored}\,(\tau) = (hc/\lambda_{\rm s})\,n\,(\tau)$. The output energy $E_{\rm out}$ is

$$E_{\rm out}\,(\tau) = \frac{F_{\rm sat}}{L_{\rm rod}}\ln\left\{1 + \left(\exp\left[\frac{E_{\rm in}}{\pi {R_{\rm s}}^2 F_{\rm sat}}\right] - 1\right)\exp\left[\sigma n\,(\tau)\,L_{\rm rod}\right]\right\} \tag{3}$$

where $F_{\rm sat}$ is the saturation fluence, $L_{\rm rod}$ is the length of the Nd:YLF rod, $R_{\rm s}$ is the seed beam's RMS radius, and σ is the emission cross section. This routine is repeated for all pulses in the train.

Table 1. Parameters of the pump and seed lasers.

Parameter	Symbol	Value
Rod length [cm]	$L_{\rm rod}$	4
Rod diameter [cm]	$D_{\rm rod}$	0.3
Pump rate [Hz]	$W_{\rm p}$	120
Pump wavelength [nm]	$\lambda_{\rm p}$	804
Fluorescence lifetime [μs]	$\tau_{\rm f}$	480
Saturation fluence [J/cm^2]	$F_{\rm sat}$	1.582
Total active ions [cm^{-3}]	$n_{\rm tot}$	1.46×10^{20}
Seed laser		
Seed wavelength [nm]	$\lambda_{\rm s}$	1053
Seed RMS radius [cm]	$R_{\rm s}$	0.08
Input energy [μJ]	$E_{\rm in}$	7
Number of pulses	$N_{\rm pulses}$	1000
Train period [ns]	$T_{\rm train}$	333

A flavor of a solution for a radially uniform beam is shown in Fig. 4a for the parameters in Table 1. The figure shows the gain $(E_{\rm out}/E_{\rm in})$ as a function of time for a train of 1000 seed laser pulses. The three typical slopes correspond to three different delay times: (i) The flat curve (green) represents a steady state, in which the amount of stored energy removed is equal to the

amount of energy increase due to the pumping between successive pulses. (ii) If the delay time is long, the stored energy may be too high before the first seed pulse enters. Therefore, the latter experiences a larger gain - this case is represented by the negative slope (red). (iii) On the other extreme, if the delay is too short, the energy reservoir is not filled up when the first seed pulse enters, and steady state gain has not yet been achieved - this case is represented by the positive slope (blue). The 'flatness' is sensitive to the delay jitter. For example, a 1% jitter in the delay time causes an order of magnitude higher spread.

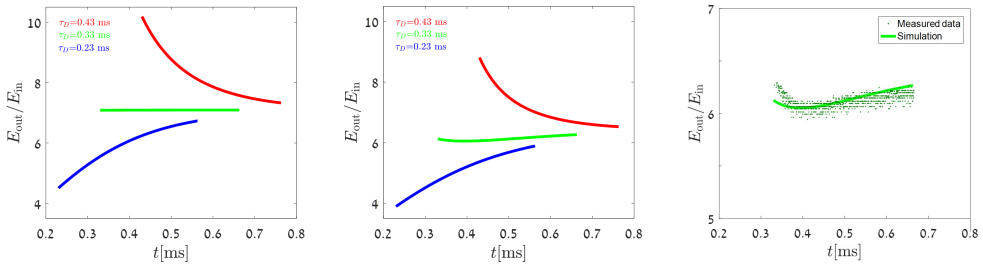

(a) Radially-uniform beam (b) Gaussian beam (c) Comparison

Fig. 4. Beam's gain for 1000 seed laser pulses as a function of time, for three different delay times, the parameters listed in Table 1 and two beam shapes: (a) Radially-uniform beam and (b) Gaussian beam. In the positive (blue) or negative (red) slopes, steady state (green) has not yet been achieved. (c) A comparison between the steady state curve (green) for the Gaussian beam from Fig. 4b, and the envelope of the measured data (green dots) from Fig. 3.

The above model for uniform beam does not explain our experimental results shown in Fig. 3, wherein there is a curvature in the steady state "flat" gain. Therefore, in what follows we present an analysis for a Gaussian beam. Figure 4b shows the gain for Gaussian beam and three delay times as in Fig. 4a. It is evident that the typical slopes (positive - blue, negative - red, steady state - green), corresponding to the three different delay times, remain the same. However, the steady state "flat" output case (green) has a curvature due to the Gaussian shape (the spread on the train is smaller than 1%). This behavior is consistent with the experimental data as seen in Fig. 4c, which shows the steady state curve (green) for the Gaussian beam from Fig. 4b, and the envelope of the measured data (green dots) from Fig. 3. While reasonable quantitative agreement is shown, further data is required in order to investigate the discrepancy between the measured data and the simulation. Such a discrepancy might stem from experimental conditions that were ignored in the simulation, such as non-uniform pump intensity, and fluctuations in the seed input energy. In the next section we discuss the reason for the curvature, and suggest ways to compensate for it.

4. Discussion

In this section we discuss the "flat" output's curvature of the Gaussian beam model in detail. The Gaussian beam is segmented into four concentric rings, as shown in the insert in Fig. 5a. Each ring has a different input fluence, since the latter depends on the effective area of the ring. We further neglect coupling between rings, and we solve Eqs. 1-3 for each ring separately.

Figure 5a shows the output energy for the Gaussian beam as a function of time, for four concentric rings. Each ring yields different types of slopes: ring 1 and 2 (beam's center) present negative slopes, whereas ring 4 (beam's edge) presents a positive slope. In between (ring 3) there is a steady state gain. The sum of the rings never yields a steady state for the whole train, but rather produces the curvature "flat case" (green curve in 4b). This curvature effect does not exist for the radially-uniform case presented in section 3.

Optics EXPRESS

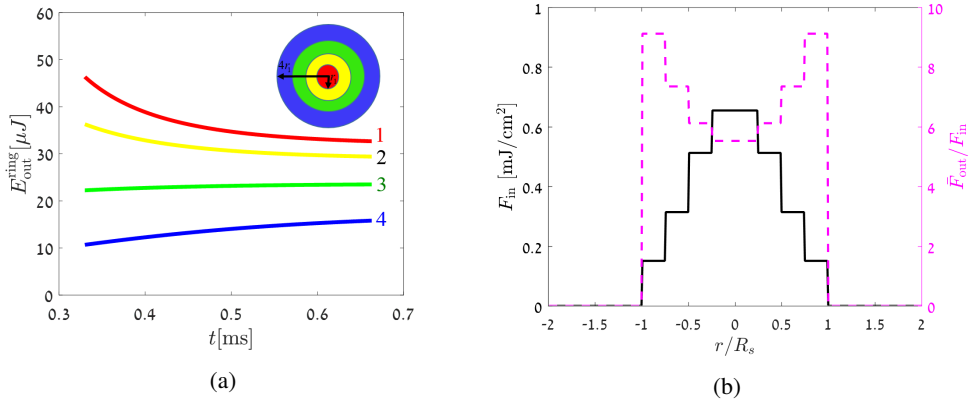

Fig. 5. (a) Output energy for the Gaussian beam as a function of time, for four concentric rings, shown in the small insert; each ring yields a different type of slope, whereas their sum yields the steady state nearly flat case (green curve in 4b). (b) Input fluence (solid black) and averaged beam gain on time (dashed pink) as a function of the radial location. Although the input fluence is the highest in the beam's center, the corresponding gain is the lowest.

Figure 5b shows the input fluence (solid black) and averaged beam gain on time (dashed pink), as a function of the radial location. Although the input fluence is the highest in the beam's center (corresponds to the red curve in Fig. 5a), the resulting averaged gain over time ($\bar{F}_{\rm out}/F_{\rm in}$) is the lowest. Further investigations showed that the curvature on the "flat" output is more pronounced for higher input energies, and mostly effected by the inner ring. Moreover, the output energy and its standard deviation does not change with the number of rings; four rings satisfy an energy spread smaller than 1%.

Lastly, our ring analysis was verified in the experiment, as seen in Fig. 6. An example of the data, broken into three different regions of the beam, corresponding to rings 1, 3, and 4, shows the output energy of a train of 1000 seed laser pulses as a function of time. Each of the regions is normalized to the first pulse's output energy $E_{\rm out}^{\rm Ring}(t = \tau_D)$. The solid curves represent the simulation results shown in Fig. 5a, and the gray dots represent the corresponding measured data. It is evident that the relative energy gain of the core decreases through the 1000-pulse train (Fig. 6a), while moving outward through the transverse beam profile, the gain is nearly flat, and it eventually begins to increase through the pulse train (Figs. 6b and 6c respectively).

While qualitative agreement is achieved for the three rings presented, reasonable quantitative agreement is shown only for the beam's center and third ring. The discrepancy between the measured data and the simulation of the fourth ring might explain some of the mis-match shown in Fig. 4c. Alternatively, it could indicate that coupling between the rings must be taken into account in the model.

Finally, there are several ways to produce a steady state uniform gain for the long train (without any curvature). First, one can utilize only part of the beam's cross section that facilitates flat gain (third ring in our analysis). Second, by employing a double pass amplifier or by flipping the signal before the next amplification component. Third, by shaping the pump current or by inserting a tapered input energy in order to cancel the curvature. Nevertheless, some applications could benefit from the non-uniform gain. For example, for accelerating a train of electron micro-bunches [11], a tapered laser pulse (as in Fig. 6c) is required in order to compensate for beam loading effect.

Optics EXPRESS

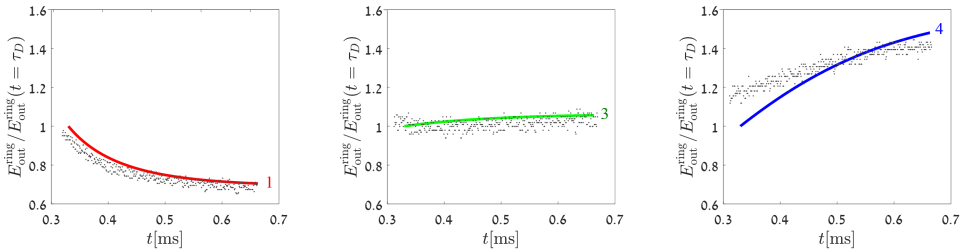

(a) Beam's center (b) Beam's third ring (c) Beam's edge

Fig. 6. Each ring's output energy normalized to the first pulse's output energy $E_{\rm out}^{\rm Ring}(t=\tau_D)$, as a function of time provides a set of relative intensity profiles for each region: (a) for the beam core (ring 1), (b) for the intermediate region (ring 3), (c) and for the outer/edge region (ring 4). The solid curves represent the simulation results shown in Fig. 5a, and the gray dots represent the corresponding measured data. The transverse laser beam's profile is shown in Fig. 2a, and its RMS radius is 0.08 cm.

5. Conclusion

The diode-pumped solid state amplifier chain at FAST Facility has been improved to have nearly flattened energy along long laser train (1000 pulses). Although the focus of this study was the flatness of the seed beam's temporal profile, the overall gain was improved from 3 to 7 for 1000 seed laser pulses, with pulse output energies of approximately 50 μJ per pulse. Increased gain results in higher yield from the photocathode, allowing for higher electron bunch intensities [2].

Through pump diode timing adjustments, we showed that uniformly amplified output for a train of seed pulses cannot be achieved. However, there is a case where the output is nearly flat, with a small curvature (the spread on the train is smaller than 1%). In order to explain our results, we suggested an analytical model accounting for the transverse Gaussian beam shape. Uniform laser pulse trains are important for applications with accelerators, where such lasers are used to produce the electron beam, and to seed or use it in pump-probe configurations.

Funding

United States-Israel Bi-national Science Foundation (BSF), the Rothschild Caesarea Foundation, Israel Science Foundation (ISF), and the U.S. Department of Energy, Office of Science, Office of High Energy Physics, under Contract No. DE-AC02-07CH11359.

References

1. P. H. Bucksbaum, "The future of attosecond spectroscopy," Science **317**, 766–769 (2007).
2. I. Will, A. Liero, D. Mertins, and W. Sandner, "Feedback-Stabilized Nd : YLF Amplifier System for Generation of Picosecond Pulse Trains of an Exactly Rectangular Envelope," IEEE J. Quantum Electron. **34**, 2020–2028 (1998).
3. I. Will, H. I. Templin, S. Schreiber, and W. Sandner, "Photoinjector drive laser of the FLASH FEL," Opt. Express **19**, 23770–23781 (2011).
4. T. Südmeyer, S. V. Marchese, S. Hashimoto, C. R. Baer, G. Gingras, B. Witzel, and U. Keller, "Femtosecond laser oscillators for high-field science," Nat. Photonics **2**, 599–604 (2008).
5. M. Herrmann, M. Haas, U. D. Jentschura, F. Kottmann, D. Leibfried, G. Saathoff, C. Gohle, A. Ozawa, V. Batteiger, S. Knünz, N. Kolachevsky, H. A. Schüssler, T. W. Hänsch, and T. Udem, "Feasibility of coherent xuv spectroscopy on the 1 S -2 S transition in singly ionized helium," Phys. Rev. A **79**, 052505 (2009).
6. S. Antipov, D. Broemmelsiek, D. Bruhwiler, D. Edstrom, E. Harms, V. Lebedev, J. Leibfritz, S. Nagaitsev, C. Park, H. Piekarz, P. Piot, E. Prebys, A. Romanov, J. Ruan, T. Sen, G. Stancari, C. Thangaraj, R. Thurman-Keup, A. Valishev, and V. Shiltsev, "IOTA (Integrable Optics Test Accelerator): facility and experimental beam physics program," J. Instrumentation **12**, T03002 (2017).

Optics EXPRESS

7. D. Mihalcea, A. Murokh, P. Piot, and J. Ruan, "Development of a Watt-level gamma-ray source based on high-repetition-rate inverse Compton scattering," Nucl. Instruments Methods Phys. Res. Sect. B: Beam Interactions with Mater. Atoms **402**, 212–215 (2017).
8. J. Li, R. Tikhoplav, and A. C. Melissinos, "Performance of the upgraded laser system for the Fermilab-NIU photoinjector," Nucl. Instruments Methods Phys. Res. Sect. A: Accel. Spectrometers, Detect. Assoc. Equip. **564**, 57–65 (2006).
9. "Proposal for an Accelerator R&D User Facility at Fermilab's Advanced Superconducting Test Accelerator (ASTA), Fermilab-TM-2568," Tech. Rep. October (2013).
10. G. J. Doster and R. Feeler, "Laser Pulse Train Amplification with PowerPULSE Modules," (2011).
11. A. Hanuka and L. Schächter, "Optimized operation of dielectric laser accelerators: Multibunch," Phys. Rev. Accel. Beams **21**, 064402 (2018).